RESEARCH ARTICLE

Lipid droplet-associated proteins in alcohol-associated fatty liver disease: A proteomic approach

Sathish Kumar Perumal[1,2] | Le Z. Day[3] | Madan Kumar Arumugam[1,2,4] | Srinivas Chava[1,2] | Vikas Kumar[5,6] | Natalia A. Osna[7] | Jon Jacobs[3] | Karuna Rasineni[1,8] | Kusum K. Kharbanda[1,2,8]

[1]Research Service, Veterans Affairs Nebraska-Western Iowa Health Care System, Omaha, Nebraska, USA

[2]Department of Internal Medicine, University of Nebraska Medical Center, Omaha, Nebraska, USA

[3]Biological Sciences Division and Environmental Molecular Sciences Laboratory, Pacific Northwest National Laboratory, Richland, WA, USA

[4]Centre for Molecular and Nanomedical Sciences, Sathyabama Institute of Science and Technology, Chennai, Tamil Nadu, India

[5]Department of Genetics Cell Biology and Anatomy, University of Nebraska Medical Center, Omaha, Nebraska, USA

[6]Mass Spectrometry and Proteomics Core Facility, University of Nebraska Medical Center, Omaha, Nebraska, USA

[7]Department of Pharmacology and Experimental Neuroscience, University of Nebraska Medical Center, Omaha, Nebraska, USA

[8]Department of Biochemistry & Molecular Biology, University of Nebraska Medical Center, Omaha, Nebraska, USA

Correspondence
Kusum K. Kharbanda, Research Service (151), Veterans Affairs Nebraska-Western Iowa Health Care System, 4101 Woolworth Avenue, Omaha, NE 68105, USA.
Email: kkharbanda@unmc.edu

Abstract

Background: The earliest manifestation of alcohol-associated liver disease (ALD) is steatosis characterized by deposition of fat in specialized organelles called lipid droplets (LDs). While alcohol administration causes a rise in LD numbers in the hepatocytes, little is known regarding their characteristics that allow their accumulation and size to increase. The aim of the present study is to gain insights into underlying pathophysiological mechanisms by investigating the ethanol-induced changes in hepatic LD proteome as a function of LD size.

Methods: Adult male Wistar rats (180–200 g BW) were fed with ethanol liquid diet for 6 weeks. At sacrifice, large-, medium-, and small-sized hepatic LD subpopulations (LD1, LD2, and LD3, respectively) were isolated and subjected to morphological and proteomic analyses.

Results: Morphological analysis of LD1-LD3 fractions of ethanol-fed rats clearly demonstrated that LD1 contained larger LDs compared with LD2 and LD3 fractions. Our preliminary results from principal component analysis showed that the proteome of different-sized hepatic LD fractions was distinctly different. Proteomic data analysis identified over 2000 proteins in each LD fraction with significant alterations in protein abundance among the three LD fractions. Among the altered proteins, several were related to fat metabolism, including synthesis, incorporation of fatty acid, and lipolysis. Ingenuity pathway analysis revealed increased fatty acid synthesis, fatty acid incorporation, LD fusion, and reduced lipolysis in LD1 compared to LD3. Overall, the proteomic findings indicate that the increased level of protein that facilitates fusion of LDs combined with an increased association of negative regulators of lipolysis dictates the generation of large-sized LDs during the development of alcohol-associated hepatic steatosis.

Conclusion: Several significantly altered proteins were identified in different-sized LDs isolated from livers of ethanol-fed rats. Ethanol-induced increases in specific proteins that hinder LD lipid metabolism led to the accumulation and persistence of large-sized LDs in the liver.

KEYWORDS
ethanol, fusion, hepatic steatosis, IPA analysis, lipid droplets, lipolysis

INTRODUCTION

The worldwide health burden attributed to alcohol is rising, and there is a robust link between population alcohol intake and liver-related fatalities (Subramaniyan et al., 2021). Alcohol-associated liver disease (ALD) refers to the damage caused to the liver by excessive consumption of alcohol. The spectrum of ALD ranges from simple steatosis (accumulation of hepatic fat) to alcoholic steatohepatitis, characterized by significant hepatic inflammation and defined histological features like hepatocellular ballooning and neutrophil infiltrations. Severe cases may result in fibrosis, cirrhosis, or even hepatocellular carcinoma (Schulze & Ding, 2019).

Hepatic steatosis, the earliest and most common hepatic response to chronic alcohol consumption, is characterized by accumulation of fat in specialized cytoplasmic organelles called lipid droplets (LDs) (Arumugam et al., 2020, 2023; Kharbanda et al., 2012; Listenberger et al., 2018). LDs are ubiquitous organelles for lipid storage and are composed of a neutral lipid core made of triglycerides and cholesterol esters bounded by a phospholipid monolayer coated with proteins (Xu et al., 2018). The monolayer-associated proteins affect LD positioning inside the cell and their association with other organelles including the rapid and dramatic changes in LD size (Kimmel & Sztalryd, 2016; Moore et al., 2005; Reue, 2011; Sharma, 2022). There is tremendous variability in LD size with diameters that range from as small as 20–40 nm to as large as 100 μm in different tissues but can also vary within the same cell type under different pathophysiological conditions (Thiam et al., 2013; Zweytick et al., 2000). This is especially evident in the liver as the small LDs observed in normal liver cells increase in size and number during the development of hepatic steatosis (Arumugam et al., 2020, 2023; Kharbanda et al., 2012; Listenberger et al., 2018; Rasineni et al., 2014). It has been suggested that LD size may influence metabolic processes including the rate of lipolysis, oxidation of fatty acids (Fei et al., 2011), as well as the capacity of the autophagic machinery to degrade entire organelles (Schott et al., 2019). Recent mechanistic studies from our laboratory have revealed that the alcohol-induced methylation defects by altering the ratio of the major phospholipids in the LD monolayer cause the accumulation of predominantly large-sized LDs interspersed with smaller-sized LDs in hepatocytes (Arumugam et al., 2020, 2023; Listenberger et al., 2018; Renier et al., 2023). To extend these investigations, our goal for this study was to isolate the LDs from livers of ethanol-fed rats to investigate whether the proteomic changes associated with the different-sized LD fractions could provide insights into underlying pathophysiological mechanisms in the development of alcohol-associated fatty liver disease. For this study, we employed label-free quantitative proteomics analyses using electrospray ionization-tandem mass spectrometry on the three different-sized LDs isolated from livers of rats fed Lieber–DeCarli ethanol diet.

MATERIALS AND METHODS

Animal experiments

Lieber–DeCarli control and ethanol liquid diets were purchased from Dyets Inc. (Bethlehem, PA). Weight-matched adult male Wistar rats (175–200 g BW), procured from Charles River Laboratories (Wilmington), were pair fed ($n = 5$) the Lieber–DeCarli control or ethanol liquid diet (Lieber & DeCarli, 1989) for 6 weeks, as described previously (Arumugam et al., 2023; Kharbanda et al., 2007). At the time of sacrifice, liver was excised and immediately processed for histology or for isolating the different-sized LD fractions. All animal care, use, and experimental procedures utilized for this study complied with NIH guidelines and were approved by the Institutional Animal Care and Use Committee of the Omaha Veterans Affairs Medical Center.

Liver histology

Formalin-fixed liver tissue was processed for hematoxylin–eosin staining and evaluated for steatosis development.

Separation and isolation of different-sized LDs

LDs of varying sizes were isolated from the liver tissues according to the protocol previously described (Zhang et al., 2016). Briefly, livers from the ethanol-fed rats were collected and rinsed with ice-cold phosphate-buffered saline (PBS). A 6 g portion of each liver was homogenized in 20 mmol/L tricine (pH 7.8), containing 250 mmol/L sucrose and 0.5 mmol/L PMSF. Each homogenate was centrifuged at 500 g for 5 min at 4°C to pellet tissue debris and blood cells. Each supernatant (8.5 mL) was transferred into ultra-clear SW 40 Ti ultracentrifuge tubes (Beckman #344059) and was overlaid with 3 mL of Buffer B (20 mmol/L HEPES (pH 7.4), 100 mmol/L KCl, and 2 mmol/L $MgCl_2$). Following

centrifugation at 500 g for 20 min at 4°C, the top white layer was collected into a 1.5 mL microcentrifuge tube and marked as large-sized LDs (LD1). Then, an equal volume of Buffer B was added back (to replace the white buffy layer just removed) and the gradient was centrifuged at 2000 g for 20 min at 4°C. The top white band was again collected into a 1.5 mL microcentrifuge tube, which was marked as medium-sized LDs (LD2). Then, another equal volume of buffer B was loaded onto the top and the gradient was centrifuged at 8000 g for 20 min at 4°C. The top white layer was again collected into a 1.5 mL microcentrifuge tube, which was marked as small-sized LDs (LD3). Finally, each LD fraction collected was further purified by centrifuging for 10 min at 4°C at the g force that was used to acquire it. The underlying solution and pellet were removed, and the LDs were gently resuspended in Buffer B. This last washing step was repeated until no pellet was visible after centrifugation. The total LD volume of each fraction was recorded, its protein content determined, and aliquots prepared for the following analysis.

Lipid extraction

Total lipids were quantitatively extracted from each LD fraction, using a modified Folch lipid extraction method (Folch et al., 1957). Triglyceride levels were biochemically determined in the lipid extract of each LD fraction, as described (Arumugam et al., 2023; Kharbanda et al., 2007, 2012).

Transmission electron microscopy (TEM)

The size of each LD fraction was examined after positive staining techniques, as detailed (Zhang et al., 2016), with the following modifications. Briefly, each LD fraction was loaded onto a Formvar-covered copper grid and sequentially fixed with 2.5% glutaraldehyde and 2% osmium tetroxide. Note that all LD fractions were used undiluted except LD1 and LD2 fractions obtained from livers of ethanol-fed rats which were appropriately diluted. The grids were stained first with 0.1% tannic acid followed by 2% uranyl acetate. Then, the grids were dried and submitted to the University of Nebraska Medical Center, Electron Microscopy Core Facility, for visualization under a FEI Tecnai G2 Spirit transmission electron microscope. ImageJ analysis was utilized to determine the average size of LDs in each fraction.

Sample preparation and LC–MS data analysis

Fifty micrograms of protein per sample underwent chloroform/methanol extraction to remove detergent. The resulting protein pellet was reconstituted in 100 mmol/L ammonium bicarbonate and subjected to overnight digestion with MS-grade trypsin (Pierce) at 37°C, preceded by reduction with 10 mmol/L DTT at 56°C for 30 min and alkylation using 50 mmol/L iodoacetamide at room temperature for 25 min. Following digestion, peptides were purified using PepClean C18 spin columns (Thermo) and reconstituted in 2% acetonitrile (ACN) and 0.1% formic acid (FA).

For analysis, 500 ng of each sample was loaded onto an Acclaim PepMap 100 75 μm × 2 cm C18 LC column (Thermo Scientific™) at a flow rate of 4 μL/min, then separated using a Thermo RSLC Ultimate 3000 (Thermo Scientific™) on a Thermo Easy-Spray PepMap RSLC C18 75 μm × 50 cm C-18 2 μm column (Thermo Scientific™). Separation was achieved with a step gradient of 4%–25% solvent B (0.1% FA in 80% ACN) from 10 to 100 min, followed by 25%–45% solvent B for 100–130 min, at a flow rate of 300 nL/min and a column temperature of 50°C, with a total run time of 155 min.

Eluted peptides were analyzed by a Thermo Orbitrap Fusion Lumos Tribrid mass spectrometer (Thermo Scientific™) in data-dependent acquisition mode. A survey full-scan MS (m/z 350–1800) was acquired in the Orbitrap at a resolution of 120,000, with an AGC target for MS1 set at 4×10^5 and an ion filling time of 100 ms. Most intense ions with charge states 2–6 were isolated every 3 s and fragmented using HCD fragmentation with 35% normalized collision energy, detected at a mass resolution of 30,000 at m/z 200. AGC target for MS/MS was set at 5×10^4 with an ion filling time of 60 ms, and dynamic exclusion was set for 30 s with a 10-ppm mass window. Each sample was analyzed in duplicate.

Protein identification was performed by searching MS/MS data against the SWISS-PROT rat protein database using the in-house PEAKS X+DB search engine. Searches were configured for full tryptic peptides with a maximum of two missed cleavage sites, including acetylation of protein N-terminus and oxidized methionine as variable modifications, and carbamidomethylation of cysteine as a fixed modification. Precursor mass tolerance threshold was set at 10 ppm, and maximum fragment mass error was 0.02 Da. The significance threshold of the ion score was calculated based on a false discovery rate of ≤1%.

Quantitative data analysis was performed using Progenesis QI Proteomics 4.2 (Nonlinear Dynamics). Raw protein intensities of each lipid droplet (LD) replicate were normalized by multiplying the normalization factor, calculated based on the volume of each LD fraction recovered, its protein content, the amount of liver used for isolating LD fractions, and the total liver weight.

Proteomic and bioinformatic analysis

Data between two groups were compared by unpaired Student's t-test, and data between multiple groups were compared by one-way analysis of variance using InfernoRDN software (available at https://www.pnnl.gov/integrative-omics). The cut-off used for the differential expression analysis summary was $p \leq 0.05$, and for the absolute fold change, the cut-off was ≥2. Principal component analysis (PCA) was conducted and visualized using RStudio Software (version 2022.07.2). Additionally, RStudio was employed for generating heat maps and volcano plots depicting differentially expressed proteins, with criteria set at an absolute Log_2Fold change >1 and a p-value ≤0.05. For further functional insights, ingenuity pathway analysis (IPA) from QIAGEN was utilized to identify enriched biological function (BF), canonical pathway categories, and regulatory networks associated with LD proteins.

Western blot analyses for validation of proteomic results

To validate the results of the IPA analysis, we conducted Western blot analyses of a few selected proteins that were differentially expressed. Immunoblotting was performed by loading equal volume of each LD fraction onto SDS-PAGE gels, as described in our publications (Arumugam et al., 2023; Kharbanda et al., 2007). The blots were incubated with primary antibodies directed against adipose differentiation-related protein/perilipin 2 (ADRP/PLIN2), perilipin 3 (PLIN3), fat-specific protein (FSP27/CIDEC), α/β hydrolase domain containing 5 (ABHD5/CGI-58), G0S2 (G0/G1 switch gene 2), adipose triglyceride lipase (ATGL), 17-beta-hydroxysteroid dehydrogenase 13 (HSD17β13), glutamate dehydrogenase 1 (GLUD1), carbamoyl-phosphate synthase 1 (CPS1), followed by the appropriate peroxidase-labeled secondary antibody. The detailed description of the source and catalog number of the primary and secondary antibodies is provided in Table S1. Proteins were visualized using standard enhanced chemiluminescence detection methods and imaged using a BIORAD ChemiDoc MP imaging system software (Bio-Rad Laboratories, Hercules, CA, USA). The intensities of immunoreactive protein bands were quantified using ImageJ software.

Immunofluorescence staining

Immunofluorescence staining for PNPLA3 was performed as described previously (Arumugam et al., 2020). Briefly, paraffin-embedded liver sections were deparaffinized in xylene and rehydrated in ethanol. Following deparaffinization, slides were subjected to antigen retrieval process with 10 mmol/L sodium citrate buffer (pH 6) at 95°C for 15 min. Blocking was done by incubating in *Super Block* (ScyTek Laboratories, AA999) for 1 hour at room temperature. Sections were incubated overnight with an antibody against Patatin-like phospholipase domain-containing protein 3 (PNPLA3; Millipore; MABS2173) overnight at 4°C. The sections were then thoroughly washed with PBS followed by incubation with ImmPRESS®-AP horse anti-rabbit IgG polymer reagent, alkaline phosphatase (Vector labs, Cat. No. MP-5401), and exposure to Vector Red Substrate Kit, alkaline phosphatase (Vector lab, cat. No. SK-5100), for signal development. Nuclei counterstaining was done by 1 µg/mL DAPI for 1 min and the slides were imaged under Keyence BZ-X810 microscope.

RESULTS

Morphological analysis of the different-sized lipid droplets

The histopathological evaluation of livers of the ethanol-fed rats was consistent with our previously published data revealing accumulation of LDs of different sizes, while there were only very few small-sized LDs in livers of control-fed rats (Figure 1A) (Kharbanda et al., 2007, 2012). The success in isolating the different-sized LDs was evident from the transmission electron microscopy images of the three fractions obtained from the liver of a representative ethanol-fed rat (Figure 1B). LD1 fraction comprised the largest-sized LDs compared with LD2 and LD3 fractions. The diameter of LDs in each image of the isolated fraction was measured by ImageJ analysis in 10 different fields to calculate the average LD size (Figure 1C).

Quantitative determination of the triglyceride content in each liver LD fraction of ethanol-fed rats revealed significant variations dependent on LD size with the highest level in LD1 fraction followed by LD2. The LD3 fraction had significantly lower amount compared with the other two fractions (Figure 1D).

LC–MS/MS analyses

Protein identifications were performed by using LC–MS/MS (Orbitrap Fusion Lumos-Thermo Scientific). After mass spectrophotometer analysis, Progenesis analysis (QI proteomics software) revealed a total of 3277 proteins across LD1, LD2, and LD3 (Tables S2A–C). To evaluate the significance of these LDs-associated proteins, principal component analysis (PCA) was performed. The PCA results revealed that LD1 (blue), LD2 (red), and LD3 (green) were clearly separated from each other (Figure 2A).

Protein expression profile of LDs

Investigation of the differentially expressed proteins between the different-sized LDs identified 1698 proteins as significantly altered ($p < 0.05$) with a fold change of >2 or <0.5 between LD1 and LD2, 641 proteins in LD2 versus LD3. and 1602 in LD1 versus LD3 (Table S2A–C). The Venn diagram investigating the overlapping proteins among the three different-sized LDs is shown in Figure 2B.

As shown in Table S3, among proteins that were significantly different between the different LD fractions, 1687 proteins were up-regulated with a fold change of >2, and 11 proteins were down-regulated with a fold change of <0.5 in LD1 versus LD2. In LD2 versus LD3, 274 proteins were up-regulated with a fold change of >2, and 367 proteins were down-regulated with a fold change of <0.5. In LD1 versus LD3, 1595 proteins were up-regulated with a fold change of >2, and 7 proteins were down-regulated with a fold change of <0.5.

Volcano plot and heat map analyses performed illustrated significantly different protein profiles of the different-sized LD isolated from ethanol-fed rats. The heat map shows the abundances of 333 proteins that were significantly different across the three different LD fractions suggesting the possibility that each LD fraction may be associated with different physiological pathways (Figure 2C).

Canonical pathway analysis

The dataset (FDR-corrected data) was analyzed using IPA core analysis to achieve a fundamental profile of the molecular processes underlying LD-associated proteins. Categorization was based on a multiple testing correction of p-value less than 0.05.

Based on the protein profile, the IPA analysis identified/predicted that the activity levels of several cellular pathways were different between the LD fractions. Here, we specifically focused on alterations in pathways related to lipid metabolism between LD1 and LD3. IPA analysis identified 373 proteins that predicted increased concentration of lipids in LD1 versus LD3. The protein details are
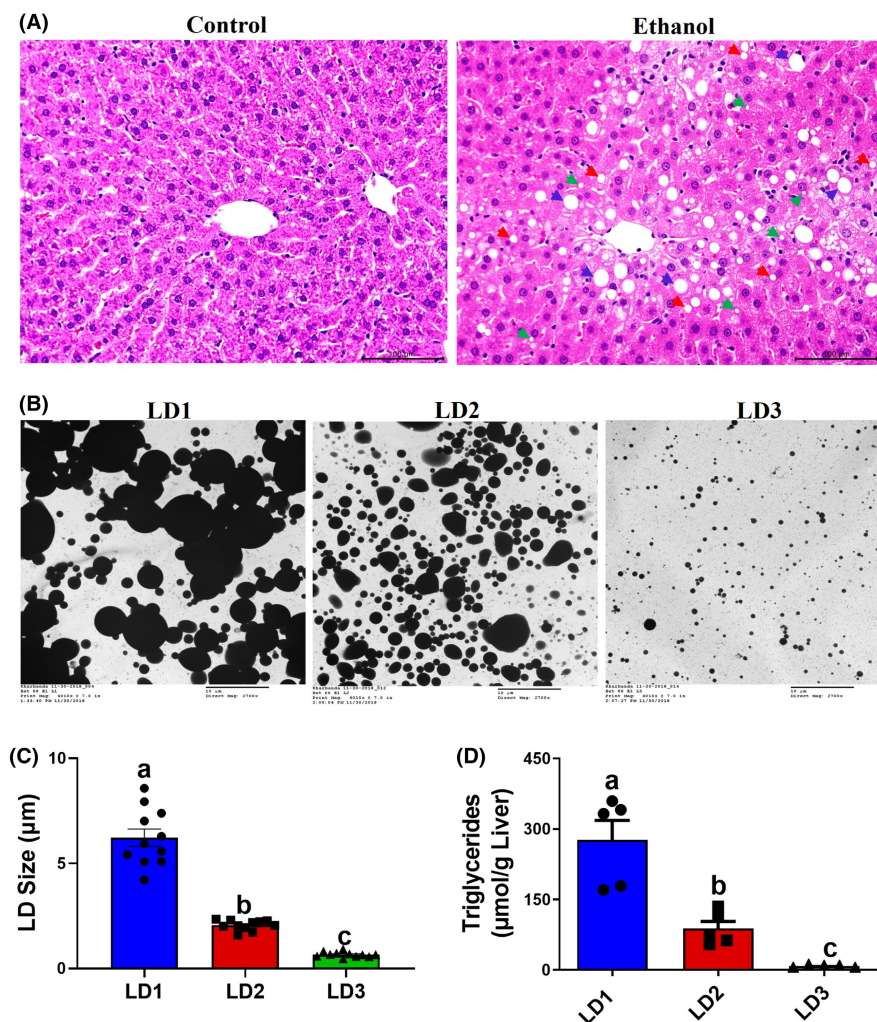

FIGURE 1 (A) Photomicrograph of hematoxylin and eosin-stained liver section of a representative control and ethanol-fed rat. The arrow marks indicate different-sized lipid droplets (LDs); Blue—LD1; Red—LD2 and Green—LD3; scale bar 100 μM; (B) transmission electron microscopy (TEM) representative images showing the morphology of different-sized LDs, scale bar 10 μM; (C) ImageJ analysis results depicting the average size of LDs in each fraction; (D) triglyceride content of each isolated LD fraction. Data are presented as the mean ± SEM (n = 5); values not sharing a common letter significantly differ from each other at p ≤ 0.05.

FIGURE 2 (A) Principal component analysis (PCA) of three different-sized LDs illustrating that protein profile of each fraction clearly separates from the others; (B) Venn diagram showing the number of proteins identified in the three different-sized LDs; (C) volcano plot and heatmap analysis of proteins identified in each LD fraction. Volcano plot illustrates that proteins are significantly different among LDs; (D) heatmap of lipid synthesis in LD1 versus LD3 derived from the IPA analysis predicting 11 pathways related to lipid synthesis is increased in LD1 than LD3. Orange color represents predicted increase, and the intensity of the coloring reflects the degree of change between the groups; (E) IPA network analysis related to uptake of lipids and incorporation of lipids in LD1 compared to LD3. Graphical representation of network analysis of proteins in LD1 versus LD3 that contributes to (1) uptake of lipids and (2) incorporation of lipids. Orange color at the center of graphical picture indicates pathway is increased. Nodes in the red color represent protein content is increased while green color represents decreased protein content. The intensity of the coloring matches with the degree of change. The orange dashed line indicates leading to activation of the pathway. Yellow dashed line represents findings that are inconsistent with the state of downstream molecule. *Represents multiple identifiers in the dataset file map to a single gene/chemical in the Global Molecular Network.

(A)

(B)

(C)

(D)

(E)

(1)

(2)
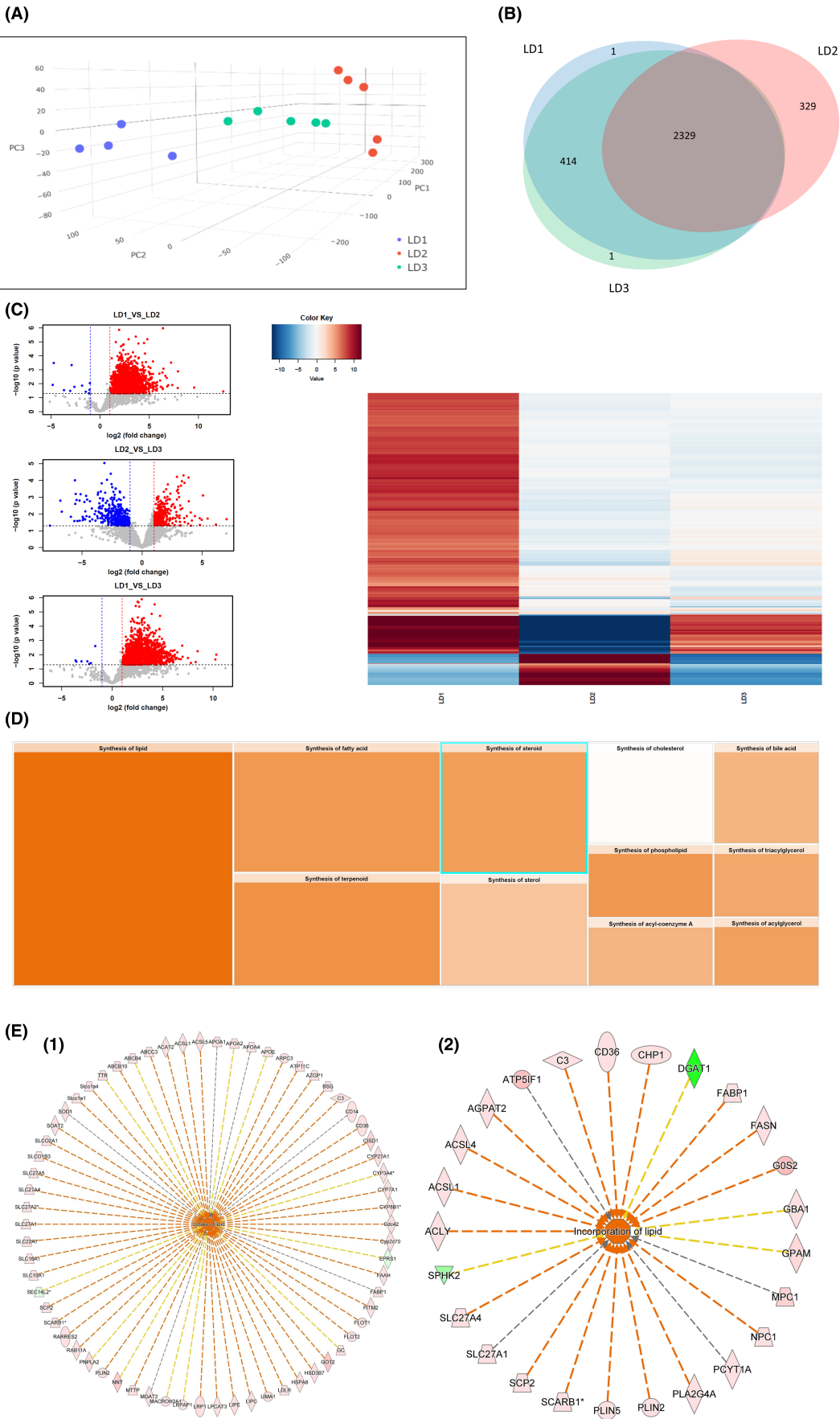
presented in Table S4. Particularly, the pathways related to lipid synthesis received a positive *Z* score (Figure 2D), indicating their activation in LD1 compared to LD3. A positive *Z* score represents predicted increase and is depicted as orange color in the heatmap analysis. The intensity of the coloring corresponds to the degree of up-regulation of the data sets. The detailed *Z*-score values and number of molecules, which are altered in each pathway of lipid synthesis, are presented in Table S5. The graphical representation of network analysis of synthesis of fatty acid is presented in Figure S1.

In addition to fatty acid synthesis, the pathways related to uptake of lipids and incorporation of lipids are highly activated and received positive *Z* scores (4.7 and 3, respectively) for LD1 compared to LD3. The graphical representation of network analysis of uptake of lipids and incorporation of lipids were presented in Figure 2E1,E2 (orange color at the center point of graphical picture represents activation of the pathway). These predictions of increased uptake and incorporation of lipids in LD1 fraction are based on increased levels of proteins involved in fatty acid transport (such as cluster of differentiation 36 (CD36), solute carrier family 27 member proteins (SLC27), and sterol carrier proteins (SCP2)) and fatty acid synthesis (such as ATP citrate lyase (ACLY), fatty acid synthase (FASN), acyl-CoA synthetase long-chain family member (ACSL4 and ACSL1), and 1-acylglycerol-3-phosphate O-acyltransferase 2 (AGPAT2)) in this fraction compared to LD3. In addition, there was a prediction for higher levels in LD1 fraction of proteins, such as PLIN2, PLIN5, and fat storage-inducing transmembrane protein 2 (FITM2), which inhibit lipolysis of the triglyceride stored within LDs by preventing the activation of lipase(s).

Validation of IPA analysis results

To validate the results of the IPA analysis, we have chosen few important proteins that were related to lipid metabolism and performed Western blot analyses followed by quantitating the band intensity. Our investigation revealed that PLIN2 protein expression levels were elevated in both LD1 and LD2 and PLIN3 expression increased in LD1 only when compared to LD3 (Figure 3A,B). We found that FSP27 was expressed only in LD1 fraction (Figure 3C,D). Furthermore, ATGL ABHD5, G0S2, HSD17β13, CPS1, and GLUD1 protein expression levels were increased in LD1 when compared to the other fractions (Figure 3C,D). Furthermore, our immunofluorescence analysis demonstrated that PNPLA3 was more prominently expressed in LD1 compared to LD3 (Figure 3G,H).

DISCUSSION

Lipid storage is not a physiological function of the liver. However, alcohol-induced imbalance among lipogenesis, influx of circulating free fatty acids, their oxidation, or the export of fat as very low-density lipoproteins (VLDL) dictates the development of hepatic steatosis, which is characterized by the accumulation of LDs in the liver (Arumugam et al., 2020, 2021; Kharbanda et al., 2007, 2012).

Research conducted in our laboratory has shed some light regarding the characteristics that allow their accumulation and size to increase with alcohol consumption (Arumugam et al., 2020, 2023; Listenberger et al., 2018; Renier et al., 2023). We have demonstrated that the accumulation of large-sized LDs is primarily dictated by the alcohol-induced increase in hepatocellular S-adenosylhomocysteine levels, which causes (i) enhanced lipogenesis, (ii) increased uptake of circulating free fatty acids from an enhanced fatty acid–binding protein expression; and (iii) decreased triglyceride breakdown from a reduction in the level of activated lipases combined with the increased expression of antilipolytic factors such as PLINs and FSP27 (Kharbanda et al., 2007, Arumugam et al., 2020, 2021, 2023). Biochemical analysis of the three different-sized LDs isolated from the livers of the ethanol-fed rats in this study revealed higher triglyceride levels in the large-sized LDs (LD1) compared to the smaller-sized LDs, LD2, and LD3 corroborating our previous study (Arumugam et al., 2023). It is well established that LD triglyceride hydrolysis to free fatty acids is a critically important prerequisite step in VLDL assembly and its secretion as well as for mitochondrial oxidation, the two processes by which the liver removes excess fat (Wiggins & Gibbons, 1992). Indeed, we had shown earlier that alcohol does impair lipolysis (Listenberger et al., 2018), which is associated with a reduced complement of activated lipases in hepatocytes (Arumugam et al., 2020). These results indicated a close association between increased triglyceride levels in the large-sized LDs with decreased lipolysis. Here, we sought to gain molecular mechanistic insights by examining the proteome and its relationship between LD size and triglyceride accumulation during the pathogenesis of ALD. The heat map data in this study clearly demonstrated the diverse intensities of proteins in three different-sized LDs in livers of ethanol-fed rats. Furthermore, the QIAGEN IPA analysis identified that the large-sized LD fraction (LD1) has higher concentration of proteins which are related to fatty acid synthesis, transport, and inhibition of lipolysis compared to smaller-sized LDs.

Regarding fatty acid synthesis, IPA analysis revealed that LD1 has more lipid/fatty acid uptake and fatty acid–synthesizing pathways activated than LD3. These predictions are based on increased concentrations of proteins for fatty acid transport proteins (CD36, SLC27, and SCP2) and fatty acid synthesis (ACLY, FSN, ACSL4, and AGPAT2). CD36, SLC27, and SCP2 are well-known fatty acid transport proteins. SLC27 gene family contains six members, and all these isoforms are involved in uptake of long-chain fatty acids. IPA identified increased concentration of SLC27A1, A2, A4, and A5 in LD1 fraction than LD3. Studies targeting SLC27 family genes in experimental animals identified that loss of SLC27 reduces long-chain fatty acid uptake in hepatocytes and triglyceride levels in the liver (Doege et al., 2008).

Regarding lipolysis, LD1 has higher protective barrier proteins (such as PLIN proteins) than LD3. This family of proteins (PLIN 1–5) is the most recognized family of LD proteins that decorates the phospholipid monolayer of LD (Greenberg et al., 1991). These proteins play important roles in LD metabolism, especially lipolysis (Kimmel et al., 2010; Listenberger et al., 2018), by protecting/
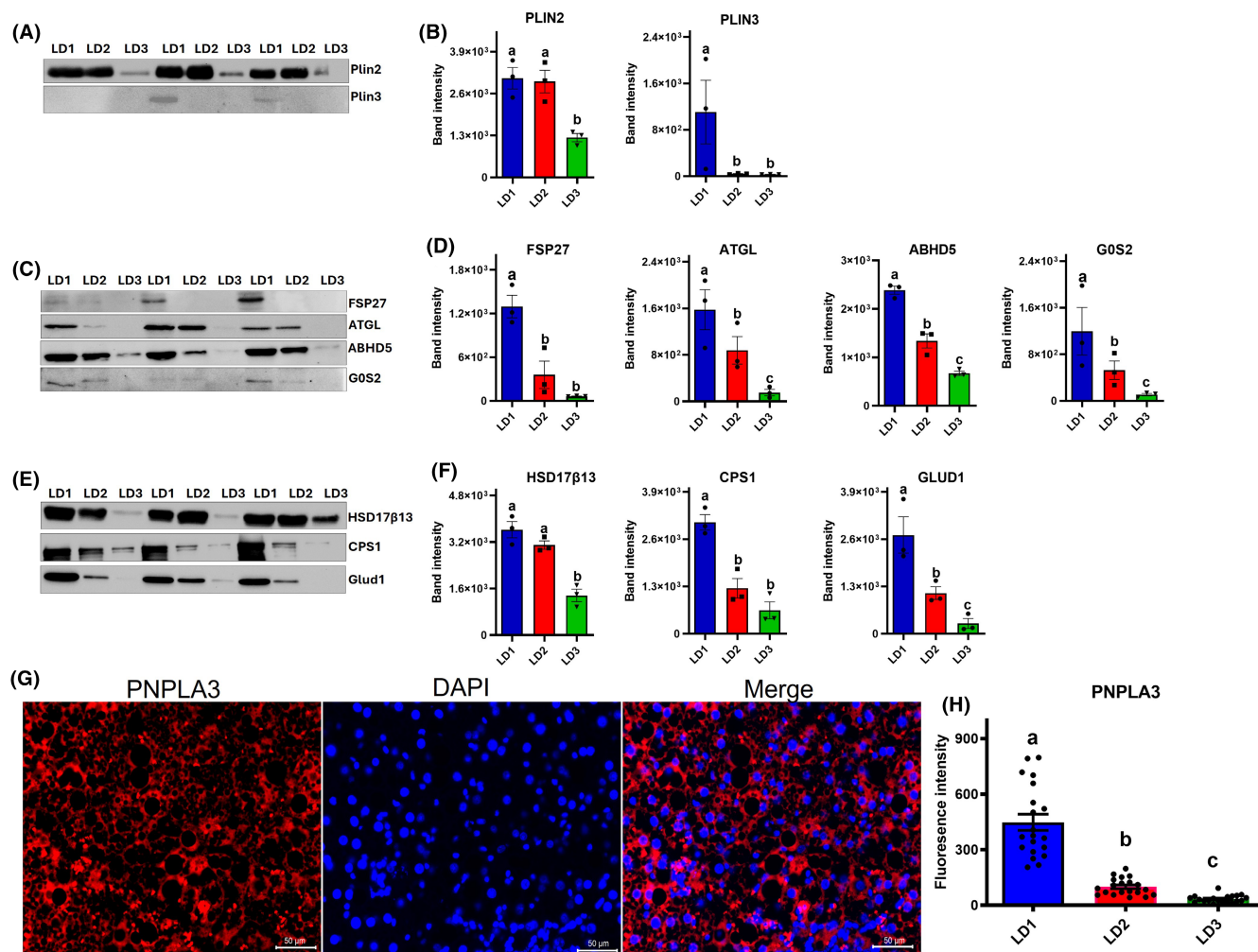
FIGURE 3 Panels (A–F) depict LDs protein quantification by Western blot and its representative graphs summarizing the intensity of immunoreactive protein bands quantified using ImageJ software. Data are presented as mean values ± SEM ($n = 3$); (G) Representative image of PNPLA3 immunofluorescent staining in livers of ethanol-fed rats; Scale bar = 50 μm; (H) The fluorescence intensity of PNPLA3 expression in different-sized LDs quantified using ImageJ software. Data are presented as the mean ± SEM from seven randomly selected fields of each section obtained from three different animals; values not sharing a common letter significantly differ from each other at $p \leq 0.05$.

shielding the LDs from lipases and subsequently causing LD growth (Sztalryd & Brasaemle, 2017). PLIN2 levels have been correlated with lipid accumulation in various tissues (Conte et al., 2016) and elevated levels of this protein have been detected in livers of ALD and MASLD animal models (Carr et al., 2014; Mak et al., 2008; Orlicky et al., 2011; Rasineni et al., 2014). Studies demonstrating a significant improvement/prevention of hepatic steatosis in the absence of these LD proteins underscore the significant role of PLIN2 and PLIN3 role in promoting hepatic steatosis (Carr et al., 2012, 2014; Chang et al., 2010). In our study, hepatic PLIN2 and PLIN3 levels were increased in LD1 when compared to LD3, implicating these proteins as a possible physiological determinant in facilitating the formation and persistence of large LDs during hepatic steatosis development.

Furthermore, we found increased level of FSP27 in LD1 compared to LD2 or LD3. This protein shares many features characteristic of PLIN proteins, including the ability to enhance neutral lipid accumulation

(Puri et al., 2007). Indeed, FSP27 overexpression in a variety of cell types has been shown to result in lipid accumulation and increased LD size by promoting LD fusion (Jambunathan et al., 2011). A further study suggested that FSP27-mediated LD fusion helps to form larger LDs, which limits the access of intracellular lipase to the LD surface due to decreased surface area of larger LDs (Keller et al., 2008) while another revealed that FSP27 directly interacts with ATGL and regulates its lipase activity (Grahn et al., 2014). Overall, FSP27 increase in LD1 contributes to its size and enhanced lipid accumulation by negatively regulating lipolysis.

Interestingly, we observed an increased protein expression of ABHD5 and ATGL in LD1 when compared to LD3. ABHD5 is an activator of the lipase, ATGL, and hence should theoretically enhance lipolysis of LD1 fraction and reduce its triglyceride content. However, that was not the case. We believe that the increased PLIN expression in LD1 compared to LD3 facilitates interaction with ABHD5 to prevent it from activating the lipase as reported
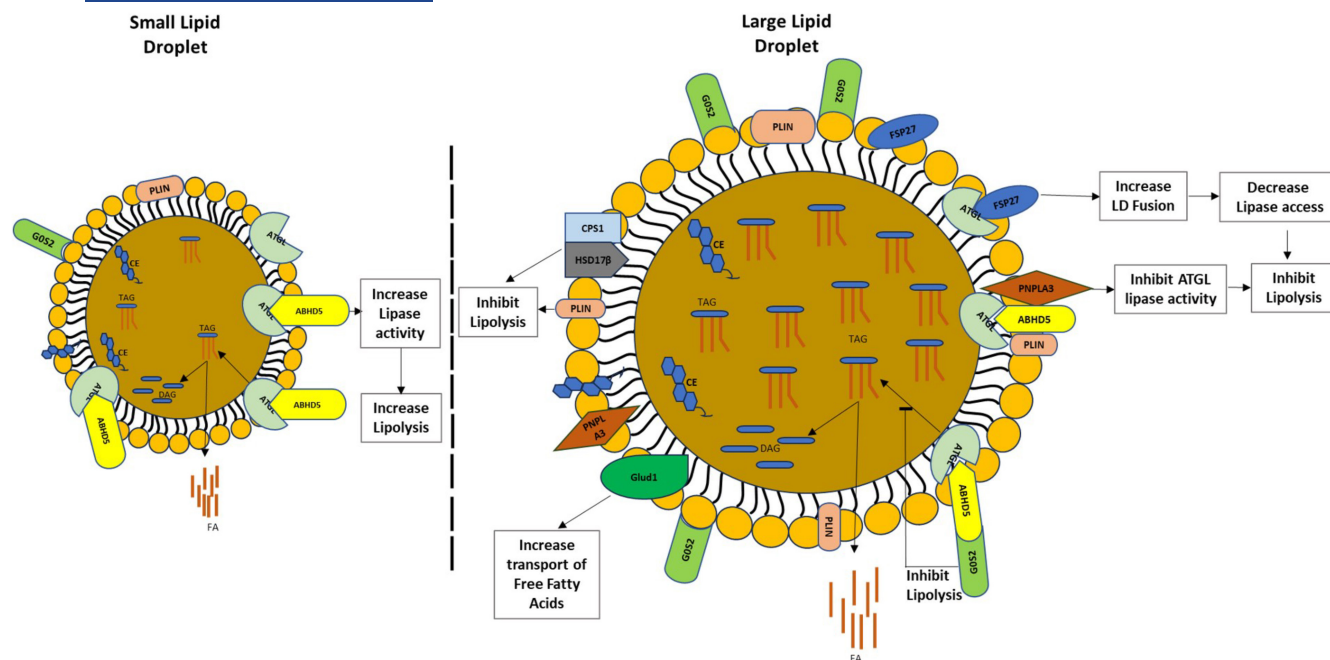
FIGURE 4 Schematic representation of the alcohol-induced proteomic changes that promote the generation of large-sized LDs and their accumulation. An increased expression of PLIN proteins on LD surface and its interaction with ABHD5 inhibits lipolysis by suppressing ATGL interaction with its activator. The G0S2 and PNPLA3 overexpression in LD1 also inhibits ATGL-mediated lipolytic activity. The increased FSP27 expression promotes fusion to generate large-sized LDs that limit the access of intracellular lipase to the LD surface due to decreased surface area of large LDs. The increased expression of HSD17β, CPS1, and GLUD1 enhances the transport of free fatty acids to promote the generation of large-sized LDs. All these changes lead to the accumulation of LD1 in the livers of rats fed the alcohol diet.

(Subramaniyan et al., 2021) and hence suppresses lipolysis of triglycerides stores of LD1.

Furthermore, we also observed an increased presence of another LD-related protein, G0S2, in LD1. This protein plays a critical role in suppressing fatty acid availability and oxidation (Heckmann et al., 2013; Heier et al., 2015; Wang et al., 2013) by directly binding to ATGL to inhibit its triglyceride hydrolase activity (Riegler-Berket et al., 2022; Yang et al., 2010). Particularly noteworthy is that G0S2, a potent inhibitor of ATGL, prevents degradation of LD triglyceride stores even in the presence of its co-activator ABHD5 (Cornaciu et al., 2011; Lu et al., 2010; Yang et al., 2010). The overexpression of G0S2 on LD1 compared to LD3 in our study suggests that despite high levels of the ATGL (and its activator) in LD1 fraction, the lipase is unable to hydrolyze triglyceride stores, thereby sustaining LD1 persistence and hepatic steatosis development.

Increased level of PNPLA3 was increased in LD1 compared to LD2 or LD3. The significant role of this LD-associated protein has mostly been provided by a genetic variant of PNPLA3 (I148M) that is associated with hepatic steatosis by slowing down triglyceride hydrolysis trapped in LDs (Basu Ray, 2019; Huang et al., 2011; Li et al., 2012; Perttila et al., 2012). Mechanistic studies have revealed that PNPLA3 reduces ATGL-mediated lipolytic activity to favor LD accumulation (Witzel et al., 2022) and based on our results, presumably the persistence of large-sized LDs.

Other critical proteins are also increased in larger LDs, such as HSD17β and CPS1. 17-Hydroxysteroid dehydrogenase is a broad family of 15 proteins that have a role in lipid metabolism that ranges

from peroxisomal fatty acid oxidation to mitochondrial fatty acid synthesis, mitochondrial β-oxidation of fatty acids, de novo cholesterol synthesis, and long-chain fatty acid elongation (Adam et al., 2018; Breitling et al., 2001; Chen et al., 2009; He et al., 1999; Jokela et al., 2010; Liu et al., 2018; Moon & Horton, 2003; Thomes et al., 2023; Venkatesan et al., 2014). Studies have demonstrated that aberrant expression of HSD17β results in accelerated LD biogenesis and excessive neutral lipid accumulation to promote fatty liver development (Casey et al., 2021; Su et al., 2014). In addition, HSD17β13 may also mediate LXRα activation-associated liver steatosis via a SREBP1-dependent mechanism (Su et al., 2017). In this study, we found the expression of different hydroxysteroid dehydrogenases, such as HSD17β4, HSD17β6, HSD17β7, HSD17β8, HSD17β10, HSD17β11, HSD17β12, and HSD17β13, was upregulated in LD1 when compared with LD3.

Regarding CPS1, our previous study showed an increase in levels of this protein in livers of ethanol-fed rats (Carter et al., 2015). Increased CPS1 levels are presumed to reflect mitochondrial damage and redox stress (Crouser et al., 2006). We observed increased CPS1 expression in LD1 relative to LD2 or LD3 in this study. How that relates to the accumulation of large-sized LDs and their persistence with alcohol administration is currently not known.

Glutamate dehydrogenase plays a key role in nitrogen and glutamate metabolism and energy homeostasis (Berry et al., 2017), and is expressed in the liver (Mao et al., 2022). Up-regulation of this protein may indicate increased transport of free fatty acids to the liver (Fernando et al., 2013). In this present study, glutamate dehydrogenase

1 (GLUD1) protein expression was up-regulated in larger LDs, which may promote increased accumulation of fatty acids and induce liver steatosis.

There are a few limitations of this study such as the sensitivity of the MS platform which limits protein detection and quantification at lower concentrations of less than 1 ng/mL. Furthermore, our comparisons between the different-sized LD fractions are limited to only those proteins that are included in the current SWISS-PROT rat database, although further searching could include any additional protein sequences or variants of interest including posttranslational modifications as appropriate. Finally, even with high-confident proteome identifications and quantification, we do recognize that the MS platform and approaches used here focus on discovery, emphasizing the identification and relative quantification of the peptides and subsequent proteins detected. As such, continued validation, either using targeted MS approaches or orthogonal antibody-based methods, that is, Western blots, as we have done here, can continue to add insight into the specific significance of many of the proteins and pathways we identified.

Other limitation of our study is analyzing only a limited number of samples ($n = 3$) for validating the proteomics results by Western blot analyses. Furthermore, while there were differences in the proteome between LD1 versus LD2 or LD2 versus LD3, as indicated in the text, an in-depth analysis was not performed as these differentiations were not as dramatic as those between LD1 and LD3.

CONCLUSIONS

In conclusion, our findings indicate that the alcohol-induced accumulation of large-sized LDs in the hepatocytes may result mainly from increased fusion and reduced lipolysis of the triglyceride stores within. Specifically, an increased expression of PLIN proteins on LD surface and its interaction with ABHD5 inhibits lipolysis by suppressing ATGL interaction with its activator. The G0S2 and PNPLA3 overexpression in LD1 also inhibits ATGL-mediated lipolytic activity. The increased FSP27 expression promotes fusion to generate large-sized LDs which limits the access of intracellular lipase to the LD surface due to decreased surface area of larger LDs. All these changes lead to the accumulation of large-sized LDs in the livers of rats fed the alcohol diet (Figure 4).

AUTHOR CONTRIBUTIONS

K.K.K.—Conception, funding acquisition, design of the study, supervision of the project, data analysis, interpretation, and final editing of the manuscript; S.K.P. and L.Z.D.—performed the experiments, data acquisition, data curation, data analysis, and writing the original draft; M.K.A. and S.C.—performed the experiments; V.K.—data curation; N.A.O. and J.J.—interpretation of the data and editing the final manuscript; K.R.—design of the study, supervision of the project, data analysis, interpretation, and final editing of the manuscript. All authors have read and agreed to the published version of the manuscript.

CONFLICT OF INTEREST STATEMENT

No conflicts of interest to declare.

DATA AVAILABILITY STATEMENT

The data generated or analyzed during this study are included in this article and as supplemental files.

ORCID

Sathish Kumar Perumal https://orcid.org/0000-0003-0151-521X
Le Z. Day https://orcid.org/0000-0002-2342-9323
Madan Kumar Arumugam https://orcid.org/0000-0003-0567-7857
Vikas Kumar https://orcid.org/0000-0001-7513-6832
Natalia A. Osna https://orcid.org/0000-0001-7498-0556
Jon Jacobs https://orcid.org/0000-0003-0557-7338
Karuna Rasineni https://orcid.org/0000-0002-9581-3957
Kusum K. Kharbanda https://orcid.org/0000-0001-7759-8889

REFERENCES

Adam, M., Heikela, H., Sobolewski, C., Portius, D., Maki-Jouppila, J., Mehmood, A. et al. (2018) Hydroxysteroid (17beta) dehydrogenase 13 deficiency triggers hepatic steatosis and inflammation in mice. *The FASEB Journal*, 32, 3434–3447.

Arumugam, M.K., Chava, S., Rasineni, K., Paal, M.C., Donohue, T.M., Jr., Osna, N.A. et al. (2021) Elevated S-adenosylhomocysteine induces adipocyte dysfunction to promote alcohol-associated liver steatosis. *Scientific Reports*, 11, 14693.

Arumugam, M.K., Perumal, S.K., Rasineni, K., Donohue, T.M., Jr., Osna, N.A. & Kharbanda, K.K. (2023) Lipidomic analysis of liver lipid droplets after chronic alcohol consumption with and without betaine supplementation. *Biology (Basel)*, 12, 462.

Arumugam, M.K., Talawar, S., Listenberger, L., Donohue, T.M., Jr., Osna, N.A. & Kharbanda, K.K. (2020) Role of elevated intracellular S-adenosylhomocysteine in the pathogenesis of alcohol-related liver disease. *Cells*, 9, 1526.

Basu Ray, S. (2019) PNPLA3-I148M: a problem of plenty in non-alcoholic fatty liver disease. *Adipocytes*, 8, 201–208.

Berry, S.A., Longo, N., Diaz, G.A., McCandless, S.E., Smith, W.E., Harding, C.O. et al. (2017) Safety and efficacy of glycerol phenylbutyrate for management of urea cycle disorders in patients aged 2months to 2years. *Molecular Genetics and Metabolism*, 122, 46–53.

Breitling, R., Marijanovic, Z., Perovic, D. & Adamski, J. (2001) Evolution of 17beta-HSD type 4, a multifunctional protein of beta-oxidation. *Molecular and Cellular Endocrinology*, 171, 205–210.

Carr, R.M., Patel, R.T., Rao, V., Dhir, R., Graham, M.J., Crooke, R.M. et al. (2012) Reduction of TIP47 improves hepatic steatosis and glucose

homeostasis in mice. *American Journal of Physiology. Regulatory, Integrative and Comparative Physiology*, 302, R996–R1003.

Carr, R.M., Peralta, G., Yin, X. & Ahima, R.S. (2014) Absence of perilipin 2 prevents hepatic steatosis, glucose intolerance and ceramide accumulation in alcohol-fed mice. *PLoS One*, 9, e97118.

Carter, W.G., Vigneswara, V., Newlaczyl, A., Wayne, D., Ahmed, B., Saddington, S. et al. (2015) Isoaspartate, carbamoyl phosphate synthase-1, and carbonic anhydrase-III as biomarkers of liver injury. *Biochemical and Biophysical Research Communications*, 458, 626–631.

Casey, C.A., Donohue, T.M., Jr., Kubik, J.L., Kumar, V., Naldrett, M.J., Woods, N.T. et al. (2021) Lipid droplet membrane proteome remodeling parallels ethanol-induced hepatic steatosis and its resolution. *Journal of Lipid Research*, 62, 100049.

Chang, B.H., Li, L., Saha, P. & Chan, L. (2010) Absence of adipose differentiation related protein upregulates hepatic VLDL secretion, relieves hepatosteatosis, and improves whole body insulin resistance in leptin-deficient mice. *Journal of Lipid Research*, 51, 2132–2142.

Chen, Z., Kastaniotis, A.J., Miinalainen, I.J., Rajaram, V., Wierenga, R.K. & Hiltunen, J.K. (2009) 17beta-hydroxysteroid dehydrogenase type 8 and carbonyl reductase type 4 assemble as a ketoacyl reductase of human mitochondrial FAS. *The FASEB Journal*, 23, 3682–3691.

Conte, M., Franceschi, C., Sandri, M. & Salvioli, S. (2016) Perilipin 2 and age-related metabolic diseases: a new perspective. *Trends in Endocrinology and Metabolism*, 27, 893–903.

Cornaciu, I., Boeszoermenyi, A., Lindermuth, H., Nagy, H.M., Cerk, I.K., Ebner, C. et al. (2011) The minimal domain of adipose triglyceride lipase (ATGL) ranges until leucine 254 and can be activated and inhibited by CGI-58 and G0S2, respectively. *PLoS One*, 6, e26349.

Crouser, E.D., Julian, M.W., Huff, J.E., Struck, J. & Cook, C.H. (2006) Carbamoyl phosphate synthase-1: a marker of mitochondrial damage and depletion in the liver during sepsis. *Critical Care Medicine*, 34, 2439–2446.

Doege, H., Grimm, D., Falcon, A., Tsang, B., Storm, T.A., Xu, H. et al. (2008) Silencing of hepatic fatty acid transporter protein 5 in vivo reverses diet-induced non-alcoholic fatty liver disease and improves hyperglycemia. *The Journal of Biological Chemistry*, 283, 22186–22192.

Fei, W., Du, X. & Yang, H. (2011) Seipin, adipogenesis and lipid droplets. *Trends in Endocrinology and Metabolism*, 22, 204–210.

Fernando, H., Wiktorowicz, J.E., Soman, K.V., Kaphalia, B.S., Khan, M.F. & Shakeel Ansari, G.A. (2013) Liver proteomics in progressive alcoholic steatosis. *Toxicology and Applied Pharmacology*, 266, 470–480.

Folch, J., Lees, M. & Sloan Stanley, G.H. (1957) A simple method for the isolation and purification of total lipids from animal tissues. *The Journal of Biological Chemistry*, 226, 497–509.

Grahn, T.H.M., Kaur, R., Yin, J., Schweiger, M., Sharma, V.M., Lee, M.J. et al. (2014) Fat-specific protein 27 (FSP27) interacts with adipose triglyceride lipase (ATGL) to regulate lipolysis and insulin sensitivity in human adipocytes. *The Journal of Biological Chemistry*, 289, 12029–12039.

Greenberg, A.S., Egan, J.J., Wek, S.A., Garty, N.B., Blanchette-Mackie, E.J. & Londos, C. (1991) Perilipin, a major hormonally regulated adipocyte-specific phosphoprotein associated with the periphery of lipid storage droplets. *The Journal of Biological Chemistry*, 266, 11341–11346.

He, X.Y., Merz, G., Mehta, P., Schulz, H. & Yang, S.Y. (1999) Human brain short chain L-3-hydroxyacyl coenzyme a dehydrogenase is a single-domain multifunctional enzyme. Characterization of a novel 17beta-hydroxysteroid dehydrogenase. *The Journal of Biological Chemistry*, 274, 15014–15019.

Heckmann, B.L., Zhang, X., Xie, X. & Liu, J. (2013) The G0/G1 switch gene 2 (G0S2): regulating metabolism and beyond. *Biochimica et Biophysica Acta*, 1831, 276–281.

Heier, C., Radner, F.P., Moustafa, T., Schreiber, R., Grond, S., Eichmann, T.O. et al. (2015) G0/G1 switch gene 2 regulates cardiac lipolysis. *The Journal of Biological Chemistry*, 290, 26141–26150.

Huang, Y., Cohen, J.C. & Hobbs, H.H. (2011) Expression and characterization of a PNPLA3 protein isoform (I148M) associated with nonalcoholic fatty liver disease. *The Journal of Biological Chemistry*, 286, 37085–37093.

Jambunathan, S., Yin, J., Khan, W., Tamori, Y. & Puri, V. (2011) FSP27 promotes lipid droplet clustering and then fusion to regulate triglyceride accumulation. *PLoS One*, 6, e28614.

Jokela, H., Rantakari, P., Lamminen, T., Strauss, L., Ola, R., Mutka, A.L. et al. (2010) Hydroxysteroid (17beta) dehydrogenase 7 activity is essential for fetal de novo cholesterol synthesis and for neuroectodermal survival and cardiovascular differentiation in early mouse embryos. *Endocrinology*, 151, 1884–1892.

Keller, P., Petrie, J.T., De Rose, P., Gerin, I., Wright, W.S., Chiang, S.H. et al. (2008) Fat-specific protein 27 regulates storage of triacylglycerol. *The Journal of Biological Chemistry*, 283, 14355–14365.

Kharbanda, K.K., Mailliard, M.E., Baldwin, C.R., Beckenhauer, H.C., Sorrell, M.F. & Tuma, D.J. (2007) Betaine attenuates alcoholic steatosis by restoring phosphatidylcholine generation via the phosphatidylethanolamine methyltransferase pathway. *Journal of Hepatology*, 46, 314–321.

Kharbanda, K.K., Todero, S.L., King, A.L., Osna, N.A., McVicker, B.L., Tuma, D.J. et al. (2012) Betaine treatment attenuates chronic ethanol-induced hepatic steatosis and alterations to the mitochondrial respiratory chain proteome. *International Journal of Hepatology*, 2012, 962183.

Kimmel, A.R., Brasaemle, D.L., McAndrews-Hill, M., Sztalryd, C. & Londos, C. (2010) Adoption of PERILIPIN as a unifying nomenclature for the mammalian PAT-family of intracellular lipid storage droplet proteins. *Journal of Lipid Research*, 51, 468–471.

Kimmel, A.R. & Sztalryd, C. (2016) The perilipins: major cytosolic lipid droplet-associated proteins and their roles in cellular lipid storage, mobilization, and systemic homeostasis. *Annual Review of Nutrition*, 36, 471–509.

Li, J.Z., Huang, Y., Karaman, R., Ivanova, P.T., Brown, H.A., Roddy, T. et al. (2012) Chronic overexpression of PNPLA3I148M in mouse liver causes hepatic steatosis. *The Journal of Clinical Investigation*, 122, 4130–4144.

Lieber, C.S. & DeCarli, L.M. (1989) Liquid diet technique of ethanol administration: 1989 update. *Alcohol and Alcoholism*, 24, 197–211.

Listenberger, L., Townsend, E., Rickertsen, C., Hains, A., Brown, E., Inwards, E.G. et al. (2018) Decreasing phosphatidylcholine on the surface of the lipid droplet correlates with altered protein binding and steatosis. *Cells*, 7, 230.

Liu, Y., Xu, S., Zhang, C., Zhu, X., Hammad, M.A., Zhang, X. et al. (2018) Hydroxysteroid dehydrogenase family proteins on lipid droplets through bacteria, *C. elegans*, and mammals. *Biochimica et Biophysica Acta - Molecular and Cell Biology of Lipids*, 1863, 881–894.

Lu, X., Yang, X. & Liu, J. (2010) Differential control of ATGL-mediated lipid droplet degradation by CGI-58 and G0S2. *Cell Cycle*, 9, 2719–2725.

Mak, K.M., Ren, C., Ponomarenko, A., Cao, Q. & Lieber, C.S. (2008) Adipose differentiation-related protein is a reliable lipid droplet marker in alcoholic fatty liver of rats. *Alcoholism, Clinical and Experimental Research*, 32, 683–689.

Mao, X., Chen, H., Lin, A.Z., Kim, S., Burczynski, M.E., Na, E. et al. (2022) Glutaminase 2 knockdown reduces hyperammonemia and associated lethality of urea cycle disorder mouse model. *Journal of Inherited Metabolic Disease*, 45, 470–480.

Moon, Y.A. & Horton, J.D. (2003) Identification of two mammalian reductases involved in the two-carbon fatty acyl elongation cascade. *The Journal of Biological Chemistry*, 278, 7335–7343.

Moore, H.P., Silver, R.B., Mottillo, E.P., Bernlohr, D.A. & Granneman, J.G. (2005) Perilipin targets a novel pool of lipid droplets for

lipolytic attack by hormone-sensitive lipase. *The Journal of Biological Chemistry*, 280, 43109–43120.

Orlicky, D.J., Roede, J.R., Bales, E., Greenwood, C., Greenberg, A., Petersen, D. et al. (2011) Chronic ethanol consumption in mice alters hepatocyte lipid droplet properties. *Alcoholism, Clinical and Experimental Research*, 35, 1020–1033.

Perttila, J., Huaman-Samanez, C., Caron, S., Tanhuanpaa, K., Staels, B., Yki-Jarvinen, H. et al. (2012) PNPLA3 is regulated by glucose in human hepatocytes, and its I148M mutant slows down triglyceride hydrolysis. *American Journal of Physiology. Endocrinology and Metabolism*, 302, E1063–E1069.

Puri, V., Konda, S., Ranjit, S., Aouadi, M., Chawla, A., Chouinard, M. et al. (2007) Fat-specific protein 27, a novel lipid droplet protein that enhances triglyceride storage. *The Journal of Biological Chemistry*, 282, 34213–34218.

Rasineni, K., McVicker, B.L., Tuma, D.J., McNiven, M.A. & Casey, C.A. (2014) Rab GTPases associate with isolated lipid droplets (LDs) and show altered content after ethanol administration: potential role in alcohol-impaired LD metabolism. *Alcoholism, Clinical and Experimental Research*, 38, 327–335.

Renier, T.J., Paetz, O.R., Paal, M.C., Long, A.B., Brown, M.R., Vuong, S.H. et al. (2023) Changing the phospholipid composition of lipid droplets alters localization of select lipid droplet proteins. *microPublication Biology*. Available from: https://doi.org/10.17912/micropub.biology.000960

Reue, K. (2011) A thematic review series: lipid droplet storage and metabolism: from yeast to man. *Journal of Lipid Research*, 52, 1865–1868.

Riegler-Berket, L., Wechselberger, L., Cerk, I.K., Padmanabha Das, K.M., Viertlmayr, R., Kulminskaya, N. et al. (2022) Residues of the minimal sequence of G0S2 collectively contribute to ATGL inhibition while C-and N-terminal extensions promote binding to ATGL. *Biochimica et Biophysica Acta - Molecular and Cell Biology of Lipids*, 1867, 159105.

Schott, M.B., Weller, S.G., Schulze, R.J., Krueger, E.W., Drizyte-Miller, K., Casey, C.A. et al. (2019) Lipid droplet size directs lipolysis and lipophagy catabolism in hepatocytes. *The Journal of Cell Biology*, 218, 3320–3335.

Schulze, R.J. & Ding, W.X. (2019) Lipid droplet dynamics in alcoholic fatty liver disease. *Liver Research*, 3, 185–190.

Sharma, A. (2022) Lipid droplets associated perilipins protein insights into finding a therapeutic target approach to cure non-alcoholic fatty liver disease (NAFLD). *Future Journal of Pharmaceutical Sciences*, 8, 1–11.

Su, W., Peng, J., Li, S., Dai, Y.B., Wang, C.J., Xu, H. et al. (2017) Liver X receptor alpha induces 17beta-hydroxysteroid dehydrogenase-13 expression through SREBP-1c. *American Journal of Physiology. Endocrinology and Metabolism*, 312, E357–E367.

Su, W., Wang, Y., Jia, X., Wu, W., Li, L., Tian, X. et al. (2014) Comparative proteomic study reveals 17beta-HSD13 as a pathogenic protein in nonalcoholic fatty liver disease. *Proceedings of the National Academy of Sciences of the United States of America*, 111, 11437–11442.

Subramaniyan, V., Chakravarthi, S., Jegasothy, R., Seng, W.Y., Fuloria, N.K., Fuloria, S. et al. (2021) Alcohol-associated liver disease: a review on its pathophysiology, diagnosis and drug therapy. *Toxicology Reports*, 8, 376–385.

Sztalryd, C. & Brasaemle, D.L. (2017) The perilipin family of lipid droplet proteins: gatekeepers of intracellular lipolysis. *Biochimica et Biophysica Acta - Molecular and Cell Biology of Lipids*, 1862, 1221–1232.

Thiam, A.R., Farese, R.V., Jr. & Walther, T.C. (2013) The biophysics and cell biology of lipid droplets. *Nature Reviews. Molecular Cell Biology*, 14, 775–786.

Thomes, P.G., Strupp, M.S., Donohue, T.M., Jr., Kubik, J.L., Sweeney, S., Mahmud, R. et al. (2023) Hydroxysteroid 17beta-dehydrogenase 11 accumulation on lipid droplets promotes ethanol-induced cellular steatosis. *The Journal of Biological Chemistry*, 299, 103071.

Venkatesan, R., Sah-Teli, S.K., Awoniyi, L.O., Jiang, G., Prus, P., Kastaniotis, A.J. et al. (2014) Insights into mitochondrial fatty acid synthesis from the structure of heterotetrameric 3-ketoacyl-ACP reductase/3R-hydroxyacyl-CoA dehydrogenase. *Nature Communications*, 5, 4805.

Wang, Y., Zhang, Y., Qian, H., Lu, J., Zhang, Z., Min, X. et al. (2013) The G0/g1 switch gene 2 is an important regulator of hepatic triglyceride metabolism. *PLoS One*, 8, e72315.

Wiggins, D. & Gibbons, G.F. (1992) The lipolysis/esterification cycle of hepatic triacylglycerol. Its role in the secretion of very-low-density lipoprotein and its response to hormones and sulphonylureas. *The Biochemical Journal*, 284(Pt 2), 457–462.

Witzel, H.R., Schwittai, I.M.G., Hartmann, N., Mueller, S., Schattenberg, J.M., Gong, X.M., Backs, J., Schirmacher, P., Schuppan, D., Roth, W. & Straub, B.K. (2022) PNPLA3(I148M) inhibits lipolysis by perilipin-5-dependent competition with ATGL. *Cells*, 12. Available from: https://doi.org/10.3390/cells12010073

Xu, S., Zhang, X. & Liu, P. (2018) Lipid droplet proteins and metabolic diseases. *Biochimica et Biophysica Acta, Molecular Basis of Disease*, 1864, 1968–1983.

Yang, X., Lu, X., Lombes, M., Rha, G.B., Chi, Y.I., Guerin, T.M. et al. (2010) The G(0)/G(1) switch gene 2 regulates adipose lipolysis through association with adipose triglyceride lipase. *Cell Metabolism*, 11, 194–205.

Zhang, S., Wang, Y., Cui, L., Deng, Y., Xu, S., Yu, J. et al. (2016) Morphologically and functionally distinct lipid droplet subpopulations. *Scientific Reports*, 6, 29539.

Zweytick, D., Athenstaedt, K. & Daum, G. (2000) Intracellular lipid particles of eukaryotic cells. *Biochimica et Biophysica Acta*, 1469, 101–120.

SUPPORTING INFORMATION

Additional supporting information can be found online in the Supporting Information section at the end of this article.